Journal of Materials Chemistry A

Accepted Manuscript

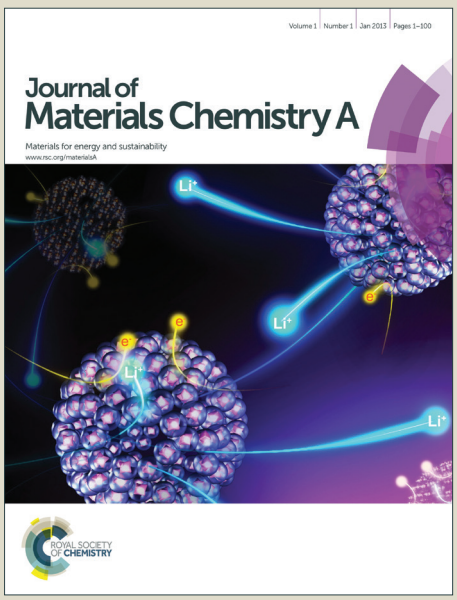

ROYAL SOCIETY OF CHEMISTRY

www.rsc.org/materialsA

The table of contents entry:

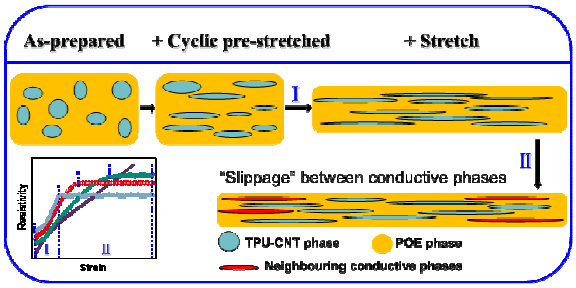

It's a new method combining polymer blends and pre-stretching to design resistivity-strain sensing conductive polymer composites. Fibrillization and "slippage" between conductive phases are proposed to explain the resistivity-strain dependency.

Journal Name

RSCPublishing

ARTICLE

Towards tunable resistivity-strain behavior through construction of oriented and selectively distributed conductive networks in conductive polymer composites

Cite this: DOI: 10.1039/x0xx00000x

Received 00th January 2012,
Accepted 00th January 2012

DOI: 10.1039/x0xx00000x

www.rsc.org/

Hua Deng,*[a] Mizhi Ji,[a] Dongxue Yan,[a] Sirui Fu,[a] Lingyan Duan,[a] Mengwei Zhang[a] and Qiang Fu*[a]

The resistivity-strain behavior of conductive polymer composites (CPCs) has gained intense interest due to its importance for various applications. The resistivity of CPCs often increases substantially and linearly under strain. To achieve constant resistivity under strain, large filler content and special network configuration are often required. And a tunable step-wise resistivity-strain behavior has yet to be reported. Herein, a new method combining polymer blends and pre-stretching is introduced to modify the resistivity-strain behavior of CPCs based on thermoplastic polyurethane (TPU)/polyolefin elastomer (POE) with multi-walled carbon nanotubes (MWCNTs) selectively incorporated in TPU phase. Depending on the compositions of blends and intensity of pre-stretching, various interesting resistivity-strain behaviors have been achieved. The resistivity can be either linearly increasing or constant. Interestingly, a two-step wise resistivity-strain behavior has been achieved, with first increase then constant. To understand this unique phenomenon, the phase morphology and conductive network structure are systematically characterized. It is observed that the orientation of MWCNTs is strongly correlated with overall resistivity. Finally, a mechanism involves fibrillization and "slippage" between conductive phases is proposed to explain the resistivity-strain dependency. This study provides a guideline for the preparation of high performance strain sensors as well as stretchable conductors.

1. Introduction

Their wide range of applications, tunable properties and ease of fabrication have made conductive polymer composites (CPCs) an interesting research topic.[1-3] With the recent emergence of large aspect ratio and multi-functional conductive fillers, such as: carbon nanotubes (CNTs)[4-8] and graphene[9-11], this area has attracted increasing amount of interest. It has been shown that the morphological control of conductive networks during the preparation of CPCs is crucial for their properties.[3, 12-17] A number of methods have been proposed to control these networks, resulting in different structural characteristics from respective morphological control methods. For instance, methods involves strong shear (such as: drawing, spinning, injection moulding, pre-straining, etc.) often lead to orientation in conductive filler;[12, 16] using polymer blends can create networks with selective distribution (with filler only distributed in one of the phases or interface in polymer blends);[13-15] thermal annealing above the melting temperature or glass transition temperature of polymer matrix can often repair conductive contacts between local conductive regions; using latex particle is able to trigger the formation of segregated networks. Furthermore, these methods can be also combined to allow the construction of conductive networks with desired special structural features.

Strain sensing as one of the most interesting applications for CPCs, has been demonstrated to have a range of applications: such as smart textile[18-20], health monitoring[7, 21, 22], wearable electronics[23, 24], movement sensor[24, 25], flexible or stretchable conductor[16, 23, 24, 26-29], etc. In these applications, different strain sensitivities or behaviors are required. For example, high sensitivity is needed for health monitoring and movement sensors; low sensitivity is essential for flexible or stretchable conductor. Therefore, it is vital to understand the resistivity-strain behavior of these CPCs. The resistivity of CPCs often increases substantially under strain. To achieve constant resistivity with increasing strain (or low strain sensitivity), it is often required to have large filler content as well as special conductive network configuration. These requirements have made the fabrication of stretchable conductors a difficult task. Therefore, it is both scientifically interesting and necessary to find alternative method for the preparation of CPCs with constant resistivity under strain. Furthermore, the resistivity of CPCs often increases linearly or almost linearly with increasing strain[30-33], other than this, step-wise change of resistivity under strain, with first increase then constant as the progress of strain, is potentially desirable for a number of intelligent applications, and can provide scientists with more optional functional "building-blocks" for the design of multi-functional materials or devices. However, a tunable two-step resistivity-strain behavior is barely reported in literature.

In our previous studies[6, 15], conductive network morphology and interfacial interaction have been shown to be crucial for the strain sensing capability of CPCs based on thermoplastic elastomer. Using various morphological control methods, such as pre-straining, thermal annealing and mixed conductive fillers etc., is shown to have significant effect on the conductive network morphology and strain sensitivity. Despite of the fact that a wide range of methods have

been demonstrated to be effective at controlling the morphology and interface of conductive network in CPCs, only few have been tested for strain sensing applications. Therefore, there is a tremendous amount of needs to explore the different strain sensing behavior of conductive networks with various characteristics in CPCs. As mentioned above, it is well known that polymer blends can trigger the formation of selectively dispersed network, and pre-straining in CPCs can often lead to orientation in conductive networks. The construction of such selectively dispersed and oriented conductive network may have profound impact on their morphology evolution under strain. As in these networks, the change of resistivity under strain is influenced by the change of network in the dispersed phases and the change of local network between these oriented conductive phases. The resistivity-strain behavior can then be tuned through adjusting these network structures. However, the network constructed through using polymer blends and subsequent pre-stretching has not been investigated, let alone the resistivity-strain behaviors of these networks.

Herein, polymer blends is used to modify the conductive network morphology in thermoplastic polyurethane (TPU)/polyolefin elastomer (POE) blends containing multi-walled carbon nanotubes (MWCNTs). Different compositions of TPU/POE blends are used with ratio in the range of: 90:10, 70:30, 50:50 and 30:70. The same overall content of 6 portions of MWCNTs is selectively incorporated in TPU phase and subsequent pre-straining process is used to modify the polymer phase structure as well as conductive network morphology in these polymer blends. The strain sensing behavior of these blends is characterized with in-line electrical measurement. To understand the strain sensing behavior, the phase morphology and conductive network structure are characterized with SEM, Raman spectroscopy and DMA. Finally, a "slippage" between conductive phases model is proposed to explain the resistivity-strain dependency observed according to the information provided by different characterization methods.

2. Experimental

2.1 Materials

Multi-walled carbon nanotubes (MWCNTs, Nanocyl 7000, Nanocyl S.A.) were used as conductive fillers in the composites. According to producer, these MWCNTs have an average diameter of 10 nm, length of 1.5 μm and a specific surface area of 250~300 m^2/g. An ethylene-octene copolymer polyolefin elastomer (POE, ENGAGE 8150) was supplied by Dow Chemical Company. Polyester based TPU (IROGRAN 455-200) was provided by Huntsman Company.

2.2 Sample Preparation

MWCNT composites were prepared in a Hakke internal mixer. All blends were mixed at 60 rpm under 160 ^oC. POE/TPU-CNT composites were melt-blended via applying two-step melt blending: MWCNTs were premixed in TPU at first and then TPU-MWCNT composites were mixed with POE in a second step. In order to minimize the possible transition of MWCNTs during the second step, these TPU-MWCNT compounds were melted in the mixer for 15 minutes while the mixing time of the second step was 5 minutes. Then, these composites were extruded as fibres with piston-mode Rosand RH70 (Malvern, Bohlin Instruments) capillary rheometer. Pre-straining of these fibres was carried out between desired strains for 25 cycles at the rate of 10 mm/min.

In this paper, samples were denoted as POE/TPU-CNT 70/30-6, representing that MWCNTs were premixed in TPU phase, containing 70 portions of POE, 30 portions of TPU and 6 portions of MWCNTs.

2.3 Characterization

Contact angles were measured in a sessile drop mould with KRUSS DSA100. Pure elastomer samples for contact angle measurements were compression moulded at 160 ^oC under 10 MPa pressure for 10 minutes then cooled to 20 ^oC. Contact angles were measured on 3ml of wetting solvent at 20 ^oC, and the results reported were the mean values of 3 replicates. The surface tensions, dispersion and polar components of these elastomers can be also obtained from contact angle measurements.

With gauge length of 50 mm, the melt-spun fibres were clamped between a pair of alumina electrodes in a SANS CMT4000 universal test machine. Electrical resistance was measured with a Keithley 6487 picoammeter under a constant voltage of 1 V to avoid strong electrical current within the sample. Resistivity can be calculated using the resistance by the following formula: $\rho=(\pi R d^2)/(4l)$, where R is the resistance of the sample, d and l represent diameter and length of the fibre sample, respectively. Both the resistance measurement set-up and tensile test machine were interfaced with a computer to record the resistance change during stretching. A constant rate of 10mm/min was used for the simultaneous resistance-strain measurement. Cyclic stretching and recovery was also conducted to investigate the dynamic resistivity-strain behavior. It should be noted that the sample with a resistivity above 105 is considered as non-conductive due to the limitation of current set-up. The initial cross sectional area under 0% strain is used to calculate the resistivity of all CPCs under different strain in this study.

Morphological studies were carried out using a scanning electron microscope (SEM, JEOL JSM-5900LV) under an accelerating voltage of 20 KV. To investigate the conductive networks below the sample surface, un-coated specimens were used (as shown in Figure 4). The conductive networks in the polymer matrix are charged to emit enriched secondary electrons to make them visible. To observe the network structure under strain, these specimens were clamped onto sample stage under different strains before observation. In addition, these fibre specimens were buried in epoxy under different strains and cryogenically fractured in a direction perpendicular to flow direction in liquid nitrogen and the fracture surfaces were coated with a thin layer of gold to examine the blend morphology and MWCNT dispersion in the composites (as shown in Figure 3 and 5).

Polarized Raman spectra was recorded on a micro-Raman spectrometer (JY HR800) equipped with a microscope. Excitation was provided by He-Ne at 786 nm. A beam size of 2 μm was used. In order to determine the orientation level of MWCNTs, the dichroism Raman spectra were achieved by recording Raman spectroscopy along two directions normal between each other, which were parallel and perpendicular to the long-axis (length) direction of fibre, respectively. All spectra were baseline corrected and the peak position and intensity were fitted in the range from 1000 cm^{-1} to 2000 cm^{-1}. The mechanism of such measurement is described in detail elsewhere in our previous studies.[6, 16]

Dynamic mechanical analysis (DMA) testing was carried out using a DMA Q800 analyzer (TA instruments, USA). The single cantilever mode was used, and the measurement was carried out on a rectangular shaped part in the size of 30mm×10.2mm×4.2mm (length × wide × thickness) from −100 to 80 °C at a heating rate of 3 °C/min and an oscillatory frequency of 1 Hz. Cooling was achieved by pumping liquid nitrogen through the accessories provided by the instrument.

3. Results and discussion

3.1 Resistivity-strain dependency of POE/TPU-CNT composites

The resistivity as a function of uniaxial strain is measured to study the strain sensing behavior of these CPC fibres. As shown in Fig. 1, the resistivity dependency on uniaxial strain of these CPCs fibres pre-stretched between different strains: a) 40-80%, b) 120-160%, c) 200-240%; is illustrated. Interesting resistivity-strain dependency is observed for these pre-stretched fibres. Increasing resistivity with increasing strain is observed for these pre-stretched fibres under initial strain. However, the same plateau is reached with increasing strain for fibres with different compositions pre-stretched under the same range of strain. Interestingly, the value of plateau is decreasing with increasing pre-stretching strain (Fig. S1). The strain at which these fibres reach plateau is decreasing with increasing pre-stretching strain. Particularly for POE/TPU CNT 70/30-6, the resistivity does not vary with strain at all if these fibres are pre-stretched between relative large strains. This unique resistivity-strain dependency is indeed very interesting and potentially important for a number of applications as mentioned above. As well known, the often observed increase of resistivity with increasing strain is attributed by the breakdown of local conductive network due to deformation. The interesting two step resistivity-strain behavior shown in Fig. 1 might indicate the formation of special network morphology. Therefore, following study is carried out to investigate the mechanism behind it.

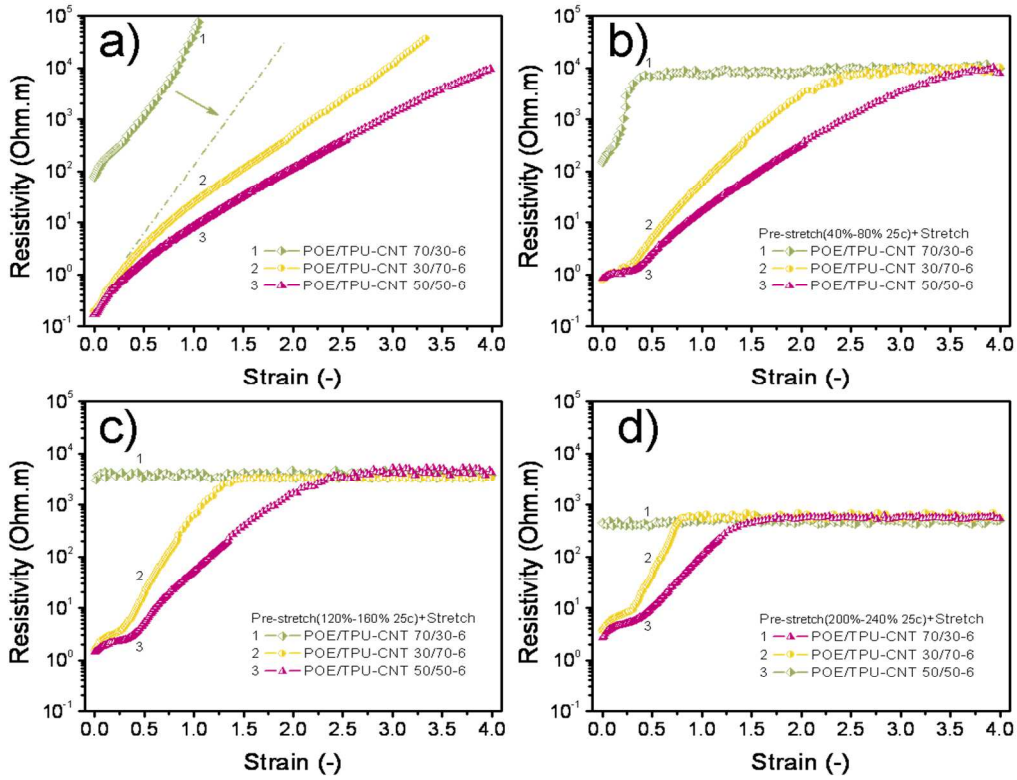

Fig. 1 Electrical resistivity strain dependency of various CPCs based on POE/TPU blends containing overall 6 wt.% of MWCNTs in TPU phase, POE/TPU blends in different ratios (70/30, 30/70, 50/50) are prepared. a) CPCs as-prepared; b) CPCs pre-stretched between 40-80% strain for 25 cycles; c) CPCs pre-stretched between 120-160% strain for 25 cycles; d) CPCs pre-stretched between 200-240% strain for 25 cycles.

To further investigate the mechanism of observed strain sensing behavior shown in Fig. 1, the recording of resistivity during pre-stretching is analyzed as shown in Fig. 2. It is clearly noted that the resistivity of POE/TPU-CNT 70/30-6 increase with increasing strain and decrease with decreasing strain during these dynamic cycles for strain between 40-80%. However, the resistivity only increases with the first increasing strain cycle and stay almost steady for the rest of dynamic cycles for larger strains (120-160%, 200-240%). This indicates the formation of special strain-resistance network morphology during the first stretching cycle at strain above 120%. This agrees with the resistivity-strain dependency observed in Fig. 1, where these two CPC fibres demonstrate almost constant resistivity with increasing strain. For the other two groups of specimens, the change of resistivity demonstrates a dynamic variation with the function of strains in different ranges (Fig. 2 a-b: 40-80%, c-d: 120-160%, e-f: 200-240%). Generally, it is observed that the resistivity of these CPCs increases with increasing strain, and decreases with decreasing strain. This is defined as positive strain effect. In addition, large shoulder peaks are observed during these cycles. In particular, the shoulder peak for strain between 40-80% is even slightly larger than the peak from positive strain effect. These shoulder peaks are regarded as indication of the competition between destruction and reconstruction of conducting pathways during dynamic loadings. The large shoulder peaks indicate strong contribution from re-construction or re-organization of conductive networks under strain. Furthermore, a gradual decrease in resistivity peak is observed during dynamic cycles, which is thought to be caused by the formation of additional conductive pathways through the breakdown and subsequent formation of interface between conductive and insulating phases (or filler and polymer matrix). The ratio between the resistivity peak of first cycle (P1, P2, P3 for 40-80% strain, 120-160% strain and 200-240% strain, respectively) and decrease of the peak value at last cycle (D1, D2, D3) as shown in Fig. 2 are listed in Table 1. Such ratio demonstrates the recovery ratio of electrical conducting ability through formation of new conductive networks during pre-stretching. It is clear that the ratio for

POE/TPU-CNT 30/70-6 and POE/TPU-CNT 50/50-6 increases from around 60% to 93% while pre-stretching strain changes from 40-80% to 200-240%. Such increase demonstrates that more conductive networks are recovered during these dynamic strain cycles at larger strains. The amplitude of these resistivity peaks under different dynamic cycles can be also obtained from Fig. 2. A general decreasing trend can be observed with increasing cycle number, indicating the formation of conductive network with more deformation resistance. The final amplitude of these CPCs is listed in Table 1, where increasing amplitude with increasing strain can be observed. This regular amplitude during cyclic stretching and increasing trend with increasing strain demonstrate these conductive networks are still sensitive to deformation in the range of 40% strain. This phenomenon agrees well with the observation shown in Fig. 1, where these CPCs are still sensitive to initial strain.

Table 1 The recovery ratio of conductive network during pre-stretching and amplitude of resistivity peak shown in Fig. 2.

POE/TPU-CNT	P_1/D_1	P_2/D_2	P_3/D_3	A_1	A_2	A_3
30/70-6	67%	91%	93%	0.73	3.94	11.16
50/50-6	59%	87%	93%	0.42	1.73	5.32

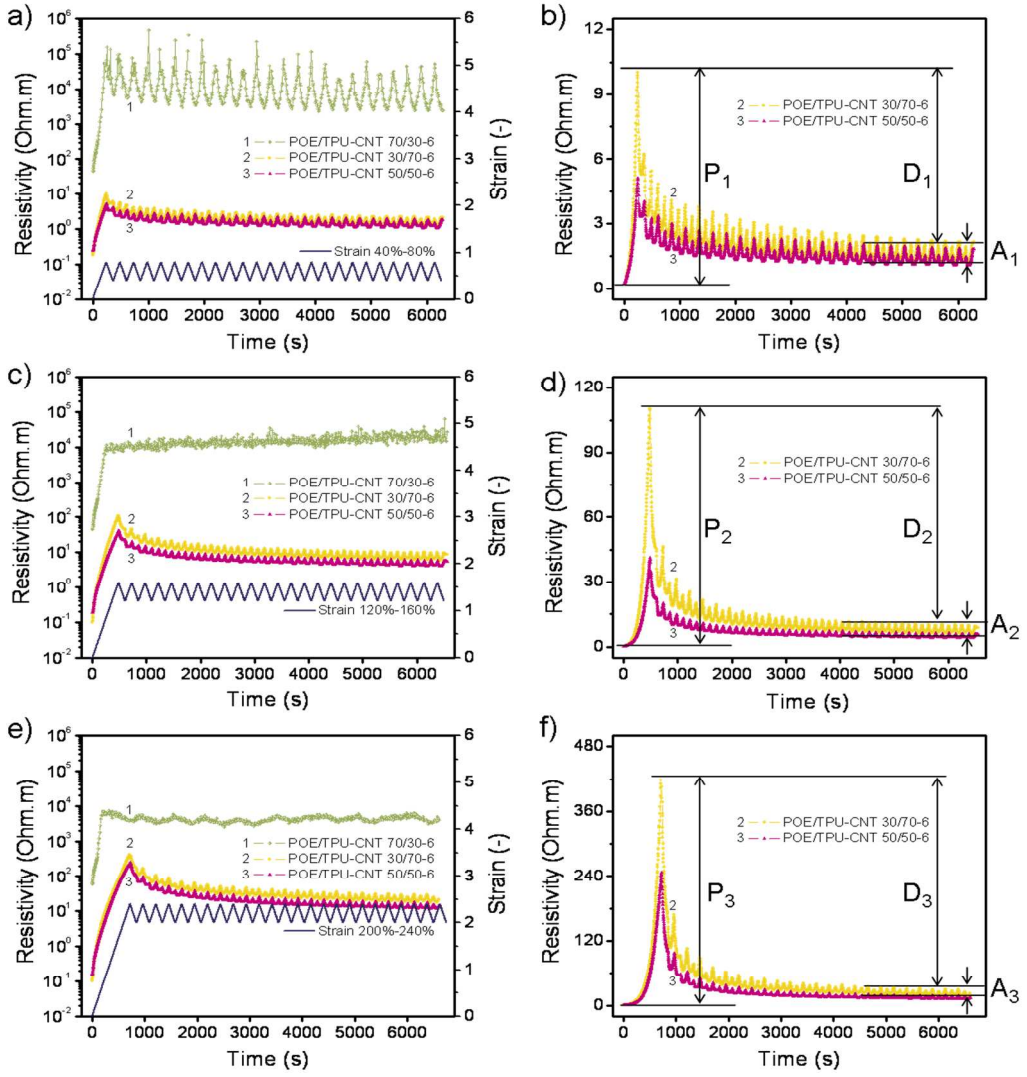

Fig. 2 The electrical resistivity of different CPCs under dynamic strain cycles in various strain range, (a, b): 40-80% strain; (c, d): 120-160% strain; (e, f): 200-240% strain.

3.2 Morphology of initial conductive networks: selective localization of MWCNTs in the blends

The electrical properties of CPCs based on polymer blends are significantly influenced by the localization of conductive fillers as well as blend morphology. As well documented in literature, the selective localization of CNTs in polymer blends can be explained by the concept of wetting coefficient.[13, 34-37] In equilibrium state, the localization of CNTs in polymer blends can be predicted by the minimization of interfacial energy. According to Young's equation, it is possible to find the equilibrium position of CNTs by evaluating the wetting coefficient ω_a, as defined in Eq. (1).[38]

$$\omega_a = \frac{\gamma_{POE-CNT} - \gamma_{TPU-CNT}}{\gamma_{POE-TPU}} \quad (1)$$

Where γ is the different interfacial energies of polymer-filler in the numerator and that of polymer-polymer in the denominator. The wetting coefficient is most commonly interpreted in a way that, for value < −1, the fillers are predicted to locate in the first polymer phase (here POE), and for value > 1, in the second polymer phase (here TPU). In the interval of ω_a value between −1 and 1, the fillers are predicted to be located at the interface.

The interfacial energies (Table 2) can be evaluated from the surface tensions of the components (obtained from contact angle measurements), using both harmonic-mean and the geometric-mean equations. The harmonic-mean equation (Eq. (2)) is valid between low-energy materials and the geometric-mean equation (Eq. (3)) is valid between a low-energy material and a high-energy material:

$$\gamma_{12} = \gamma_1 + \gamma_2 - 4\left(\frac{\gamma_1^d \gamma_2^d}{\gamma_1^d + \gamma_2^d} + \frac{\gamma_1^p \gamma_2^p}{\gamma_1^p + \gamma_2^p}\right) \quad (2)$$

$$\gamma_{12} = \gamma_1 + \gamma_2 - 2\left(\sqrt{\gamma_1^d \gamma_2^d} + \sqrt{\gamma_1^p \gamma_2^p}\right) \quad (3)$$

where γ_1, γ_2 are the surface tensions of components 1, 2; γ^d_1, γ^d_2 are the dispersive parts of the surface tensions of components 1, 2; and γ^p_1, γ^p_2 are the polar parts of the surface tensions of components 1, 2.

For these two methods, the calculated wetting coefficients are positive (and below 1, Table 2). For high aspect ratio filler carbon nanotubes, thermodynamics stable localization at the blend interface is expected to be unlikely.[14] And the interfacial energy between TPU and MWCNT ($\gamma_{TPU-CNT}$) is slightly lower than that between POE and MWCNT ($\gamma_{POE-CNT}$), which indicates a slightly better wetting of MWCNT with TPU. Therefore, the TPU-MWCNT pair tends to be formed to minimize the total free energy in the ternary composite of POE/TPU-CNT. Besides thermodynamic issues, the selective localization of CNTs in polymer blends can be also governed by kinetic factors[39-41], such as mixing procedures, mixing time, shear strength, etc. The final localization behavior of CNTs in polymer blends is mainly determined by the interplay between thermodynamic driving forces and kinetic factors.

Table 2 Interfacial energies and wetting coefficients as calculated using harmonic and geometric mean equations.

Calculation methods	Interfacial energies (mN/m)			Wetting coefficient (ω_a mN/m)	Adhesion work ($W_{polymer-CNT}$ mN/m)
	$\gamma_{POE-CNT}$	$\gamma_{TPU-CNT}$	$\gamma_{POE-TPU}$		
Harmonic mean equation	5.70	3.45	2.94	0.765	$W_{POE-CNT}$ =59.96
Geometric mean equation	2.92	1.76	1.54	0.757	$W_{POE-CNT}$ =67.73

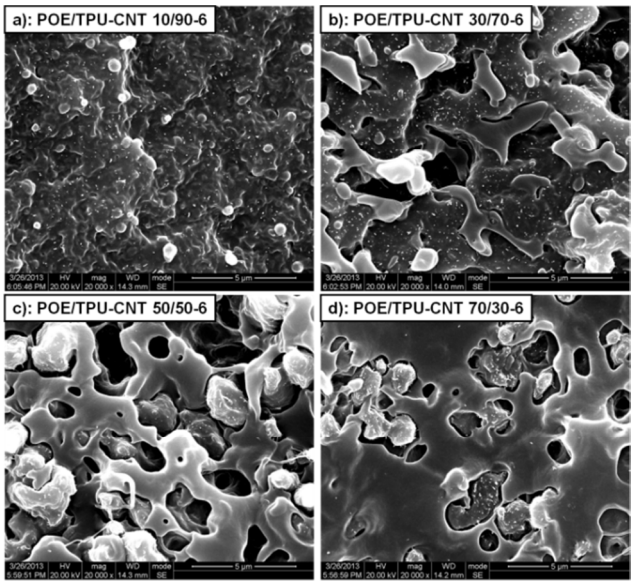

Fig. 3 SEM pictures of fracture surface from different as-prepared blends, a) POE/TPU-CNT 10/90-6, b) POE/TPU-CNT 30/70-6, c) POE/TPU-CNT 50/50-6, d) POE/TPU-CNT 70/30-6.

Thus, the pre-mixing of MWCNTs in TPU phase followed by mixing with POE phase with much short time (to minimize possible transition of MWCNTs from TPU to POE) in POE/TPU-CNT blends, can cause selective localization of MWCNTs in TPU phase. To confirm this assumption and observe their phase morphology, SEM is carried out on the fracture surface of these blends with different compositions (Fig. 3). It is observed that continuous TPU phase is formed for blends containing 90 and 70 portions of TPU. Meanwhile, it is clearly noted that MWCNTs are selectively distributed in the continuous TPU phase. For blends containing POE/TPU in the ratio of 50/50, a more or less co-continuous structure be can be observed. With further increase of POE content to 70 portion, POE phase becomes the continuous phase. In these two blends, most of the MWCNTs are still distributed in TPU phase, as indicated by the large amount of white dots in TPU phase and few in POE phase. Possible transition of small amount of MWCNTs from TPU to POE might be caused by the large relative MWCNTs content in TPU phase (17 wt.% in this case). It is worthy pointing out that it is very difficult to further reduce the content of TPU phase in this study, as dispersing an overall 6 portion of MWCNTs in such low content of TPU phase is a challenging task. Furthermore, as POE/TPU-CNT 70/30-6 still demonstrates relative low resistivity as shown in Fig. 2, it is speculated that the conductive network in that particular blend is formed through the dispersed TPU-CNTs phase in conjunction with the small amount of MWCNTs in POE phase, or these dispersed TPU-CNT phases are still connecting with each other three-dimensionally.

3.3 Morphology of conductive networks under strain

To understand the electrical property-strain dependency behavior observed above, SEM is carried out to investigate the phase morphology as well as conductive network structure. Firstly, as shown in Fig. 4, SEM using a high accelerating voltage causing MWCNTs in the insulating polymer matrix to become charged , is carried out to study the condcutive network structure. It should be noted that conductive networks buried underneath the matrix can be observed using this technique. The bright bundles in the micrographs are MWCNTs and the grey area is polymer matrix. It can be clearly observed that slightly oriented conductive networks along spinning direction are contained in as-prepared blends (a, d, g), oriented MWCNT bundles along pre-stretching direction are observed in pre-stretched fibres (b, e, h), and highly aligned MWCNTs bundles are observed in pre-stretched fibres under 200% strain (c, f, i). In these pictures, little difference is found between fibres with different

compositions. Moreover, little difference is found in terms of the selective distribution of MWCNTs either. This might be attributed to the fact that conductive network buried in the matrix can be visualized by this technique and the phase morphology of polymer blends can not.

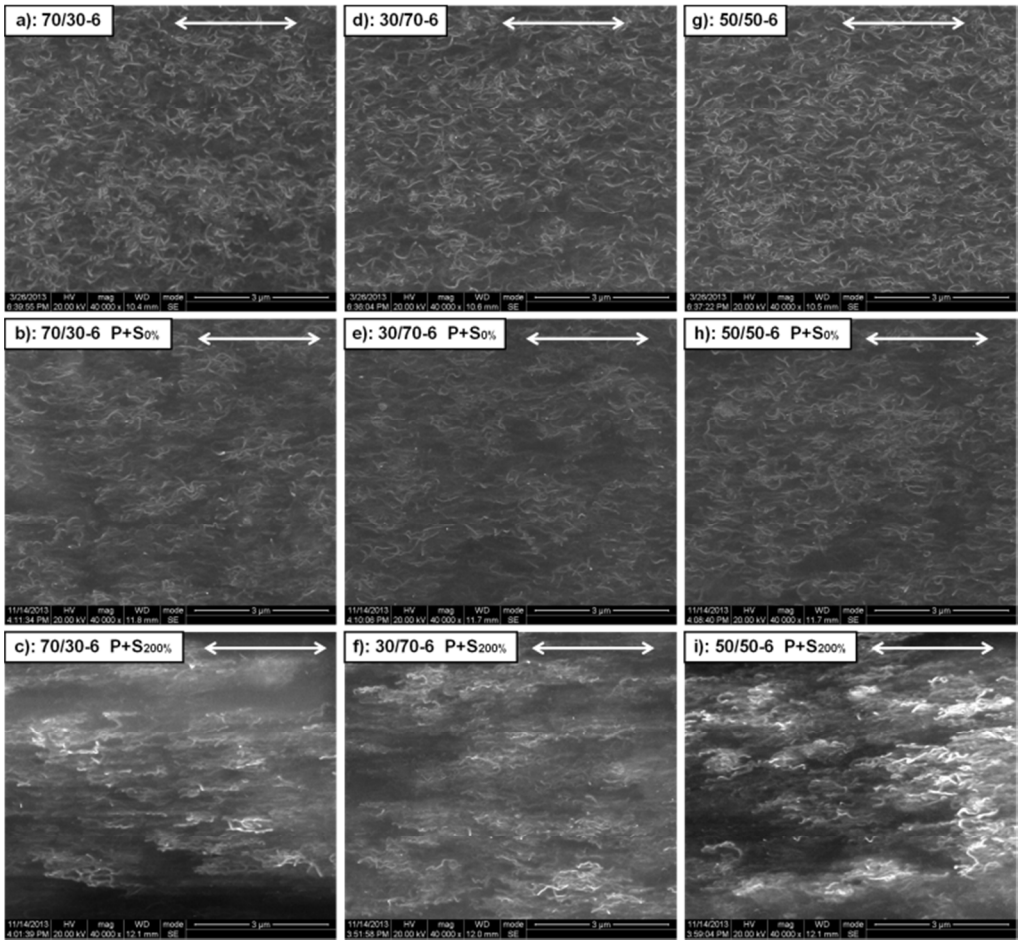

Fig. 4 SEM of conductive network structure in different CPCs, a) as-prepared POE/TPU-CNT 70/30-6, b) pre-stretched POE/TPU-CNT 70/30-6 between 120-160% strain, c) pre-stretched POE/TPU-CNT 70/30-6 between 120-160% strain under 200% strain; d) as-prepared POE/TPU-CNT 30/70-6, e) pre-stretched POE/TPU-CNT 30/70-6 between 120-160% strain, f) pre-stretched POE/TPU-CNT 30/70-6 between 120-160% strain under 200% strain; g) as-prepared POE/TPU-CNT 50/50-6, h) pre-stretched POE/TPU-CNT 50/50-6 between 120-160% strain, i) pre-stretched POE/TPU-CNT 50/50-6 between 120-160% strain under 200% strain. Please note that the arrow indicates fibre spinning or pre-stretching direction.

Table 3 Orientation factors calculated according to Raman spectra shown in Fig. 6 for different composites at various processing stages.

POE/TPU-CNT	As-prepared	P+$S_{0\%}$	P+$S_{50\%}$	P+$S_{100\%}$	P+$S_{200\%}$	P+$S_{250\%}$
70/30-6	0.915	1.459	1.493	–	1.500	–
30/70-6	0.776	1.005	1.152	1.480	1.489	1.492
50/50-6	0.573	0.734	–	1.332	1.482	1.486

Therefore, SEM on the fracture surface of these fibres under different strain is carried out to illustrate the change of phase morphology under strain, as shown in Fig. 5 and S2-S5. By comparing Fig. 3 with 5, it is observed that the isotropic phase morphology in as-prepared fibres is transformed into elongated phases by pre-stretching. It is noted that the dispersed phase, TPU phase in Fig. 3d, 5a and POE phase in Fig. 3b, 5b, still remain as dispersed phase. Moreover, the majority of MWCNTs are still distributed in TPU phase. While these blends are under 200% strain, as shown in Fig. 5b, 5d and Fig. S3, S5, these elongated dispersed phase as well as matrix phase are transformed into fibrils in the stretching direction. Therefore, considering the results mentioned above, it is clear that selectively dispersed and oriented conductive network are formed in these CPCs. In these networks, the change of resistivity is attributed by two issues: the change of network in these dispersed phases or the change of local network between these oriented conductive phases. The special configuration of such selectively distributed and oriented and conductive networks has confined the phase morphology evolution and conductive network morphology evolution under strain into few scenarios. And the overall change of conductive networks can be observed by monitor the change of overall resistivity under strain. Therefore, the information on the orientation status of MWCNTs in these networks can provide vital information on the morphology. To quantify the

orientation of MWCNTs under different strain in these CPCs, Raman spectroscopy is carried out as shown in Fig. 6 and Table 3-4. Resonance-enhanced Raman scattering effect can be observed in MWCNTs while a visible or near infrared laser is used as excitation source and such a resonance effect is not observed for polymer matrix. Therefore, Raman spectroscopy is an ideal method to characterize the orientation of MWCNTs. The two bands at around 1580 cm^{-1} and 1350 cm^{-1} in the spectra are assigned to E_{2g} and A_{1g} modes, respectively. The former is denoted as G-band generated by stretching mode of sp^2 atom pair in carbon ring or long chain and the latter is denoted as D-band induced by structure disorder and flaw. For these CPC fibres, the Raman spectra were recorded both parallel ($//$) and perpendicular to ($\perp$) the stretching direction. To evaluate the orientation degree of MWCNTs, the depolarization factor (R) was adopted, which is defined as the ratio of peak intensity for G band in the parallel direction ($I_{//}$) to that in the perpendicular direction ($I_{\perp}$), $I_{//}/I_{\perp}$. An R value close to unity indicates an isotropic morphology, whereas a value higher than unity implies preferential orientation along the stretching direction. It is understood that the beam size is slightly smaller than the phase size in these blends. However, by considering the Raman spectra can penetrate slightly into the polymer matrix, and these filler networks can still be considered randomly distributed in 3D, as shown by SEM images in Figure 4. Furthermore, systematic and stable data has been obtained in our study. Therefore, such method is suitable for this purpose.

Table 4 The orientation degree of MWCNTs obtained from Raman spectroscopy in these fibres shown in Fig. 6.

POE/TPU-CNT 30/70-6	0% strain	100% strain	250% strain
As-prepared	0.776	1.399	1.585
Pre-stretched			
Pre-stretch 1 (40%-80% 25c)	0.937	1.432	1.463
Pre-stretch 2 (120%-160% 25c)	1.005	1.480	1.492
Pre-stretch 3 (200%-240% 25c)	1.067	1.537	1.539

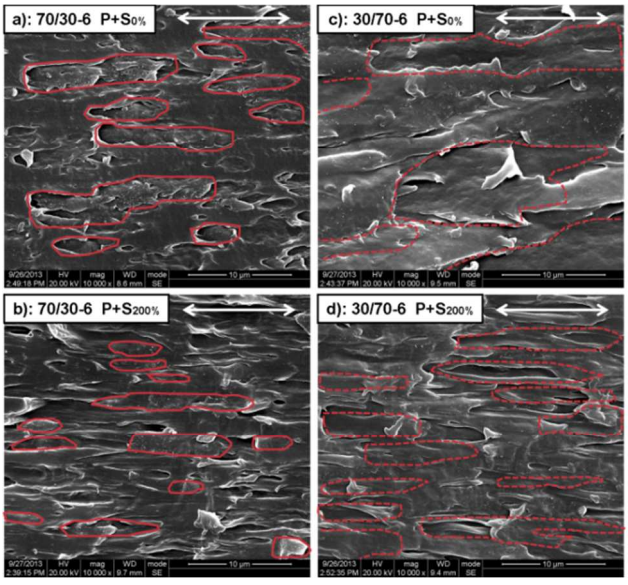

Fig. 5 SEM pictures showing the phase morphology of polymer blends, a) pre-stretched POE/TPU-CNT 30/70-6 blends between 120-160% strain, b) pre-stretched POE/TPU-CNT 30/70-6 blends between 120-160% strain under 200% strain; c) pre-stretched POE/TPU-CNT 30/70-6 blends between 120-160% strain, d) pre-stretched POE/TPU-CNT 30/70-6 blends between 120-160% strain under 200% strain. Please note that the arrows indicate stretching direction; and TPU phase containing MWCNTs are marked with solid red lines in a and b; POE phase without MWCNTs are marked with dashed red lines in c and d.

As shown in Fig. 6 and Table 3-4, the degree of orientation for MWCNTs in these blends is generally increasing with increasing strain. A maximum value of around 1.5 is reached. It is clearly noted that the strain at which the degree of orientation reaches maximum is different for CPCs with different compositions. For POE/TPU-CNT 70/30-6, the pre-stretched fibres between 120-160% strain reaches 1.459 and with little increase in the orientation of MWCNTs observed while they are under further strain. For POE/TPU-CNT 30/70-6, the pre-stretched fibres under further 100% strain reaches 1.48 and little increase in the orientation of MWCNTs is obtained while even large strain is applied. For POE/TPU-CNT 50/50-6, the pre-stretched fibres under further 200% strain reaches 1.482, and very little increase in the orientation of MWCNTs is noted while strain increases further. The dependency of MWCNTs orientation degree on strain is similar to that of the resistivity as shown in Fig. 6d. It indicates that the orientation of MWCNTs is closely related with the overall resistivity. For POE/TPU-CNT 30/70-6, the degree of orientation for MWCNTs demonstrates a similar trend with the change of resistivity under strain (list in Table 4), where the MWCNTs orientation increases almost linearly with strain for as-prepared CPCs with an orientation degree of 1.585 at 250% strain (the highest among all specimens in this study), and pre-stretched CPCs demonstrate a plateau under strain. The extra information can be provided by Table 4 is that the resistivity-strain dependency with lower plateau is shown to have higher MWCNTs orientation. It is also noted that pre-stretching at higher strains can lead to more orientation in MWCNTs at various strains.

The shear induced orientation in MWCNTs often lead to increase in resistivity due to break down of local conductive networks during orientation.[1, 15, 42] To achieve constant resistivity under large strain, special conductive network structure is often needed. As the change of resistivity in CPCs under strain relies on the change of conductive network during stretching, thus, such change should be highly dependent on the conductive network morphology in these TPU-CNT phases as well as the phase morphology in this case. By considering the above morphological observations and phenomenon shown in Fig. 6d and Table 3-4, the increase in MWCNTs orientation upon initial stretching is attributed by the fibrillization and orientation of TPU-CNT phase. Under further stretching, the overall resistivity is kept constant. As discussed above, the change of conductive networks between and within these selectively dispersed phase are responsible for the overall resistivity change. Therefore, the constant resistivity under strain indicates that stable conductive networks are obtained between

and within these networks. By considering the fact that these networks are under substantial amount of strain, it is thought that the slippage between conductive phases might be the main mechanism responsible for the observed resistivity-strain behavior, as no further increase in the MWCNTs orientation as well as resistivity can be obtained once these conductive phases are slipping between each other. It should be noted that the initial cross-section of these specimens under 0% strain are used for the calculation of resistivity (even for specimens are under 250% strain). Therefore, the above discussed resistivity can be considered as resistance and is directly related with the morphology of conductive pathways.

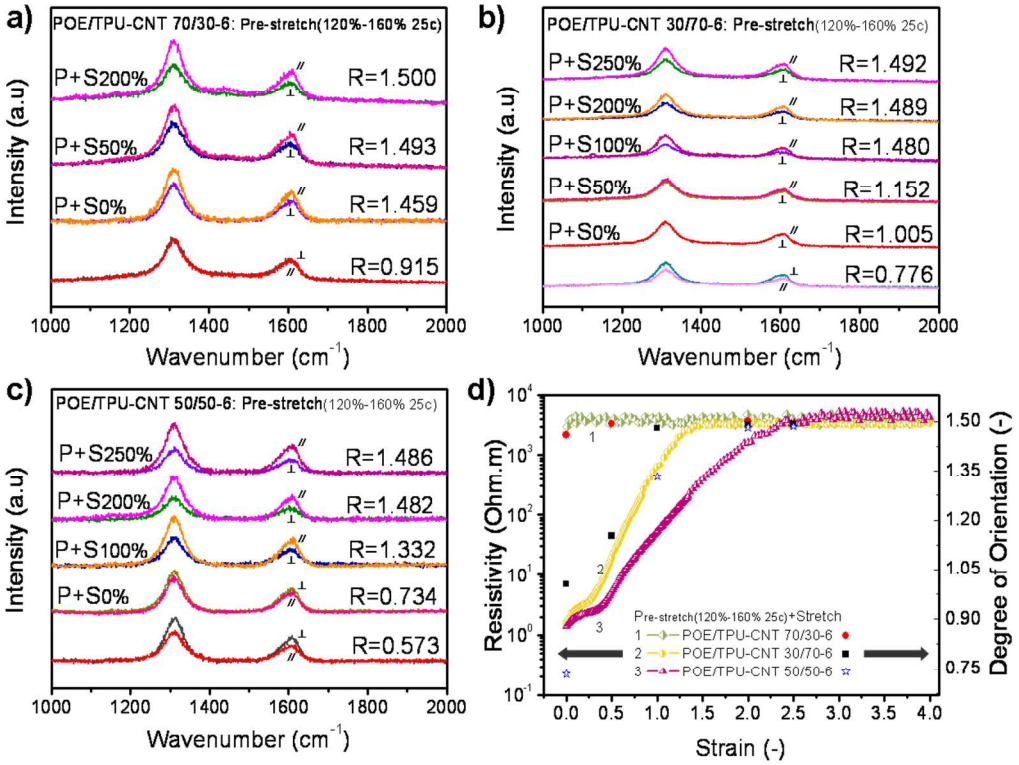

Fig. 6 Orientation measurements from Raman spectroscopy for POE/TPU-CNT 70/30-6 (a), POE/TPU-CNT 30/70-6 (b), POE/TPU-CNT 50/50-6 (d), composite fibres at different processing stages; bottom curve: as-prepared composite, P+S0%=pre-stretched, P+S50%=pre-stretched composites under 50% strain. Raman spectra (// : parallel to stretching direction; ⊥ : perpendicular to stretching direction). (d) A comparison between the dependency of resistivity as well as MWCNTs orientation on strain.

3.4 Mechanism and model

According to above results and discussion, a sketch of the polymer blends phase morphology evolution during different processing stages is drawn to describe the mechanism more vividly. As shown in Fig. 7, isotropic polymer phases in as-prepared CPCs are elongated by cyclic pre-stretching process. During such cyclic process, the almost isotropic conductive networks in these CPCs are transformed into oriented networks. With the formation of additional conductive networks during pre-stretching and releasing, these networks are more resistant to deformation as indicated by the recovery ratio of conductive network shown in Fig. 2. While these pre-stretched CPCs are under further stretching, most of the CPCs (except POE/TPU-CNT 70/30-6 pre-stretched between 120-160% and 200-240% strain) illustrate a two step wise change of resistivity with the function of strain. In the first stage as shown in Fig. 7, the elongated polymer phases are transformed into fibrils by stretching. The resistivity increases with further stretching due to the deformation of conductive phases as well as breakdown of local conductive networks between neighbouring conductive phases. This is evidenced by the enhancement in degree of MWCNTs orientation shown in Fig. 6d. In the second stage shown in Fig. 7, the resistivity is kept almost constant during further stretching, meanwhile, the degree of MWCNTs orientation also levels with increasing strain. This indicates the conductive phases in these blends are not deformed further in the second stage. Thus, the mechanism of "slippage" between conductive phases is proposed to explain the observed behavior, where the destruction of conductive networks due to slippage between conductive phases under strain is compensated by the formation of additional networks with neighbouring conductive phases (as shown in Fig. 7). It should be noted that in the case of POE/TPU-CNT 70/30-6 the first stage is only observed at relative small pre-stretching strains (40-80%). This might be caused by the relative low content of conductive phase (TPU-CNT), thus, forming elongated phases at relative larger pre-stretching strains. The further deformation of these elongated phases is relative more difficult than the blends containing 50% or 70% of TPU-CNT phase might be caused by another fact that the relative CNT content in POE/TPU-CNT 70/30-6 is much higher than the rest (17 wt.%, 11 wt.% and 8 wt.% for blends containing 30%, 50% and 70% TPU-CNT phase, respectively). Thus, the modulus of these TPU-CNT phases should be higher leading to a more stable morphology of individual phase during stretching. To confirm this assumption, DMA test was carried out as shown in Fig. S6. The storage modulus of these materials at 20 ^{o}C can be used to calculate the effective modulus of these TPU-CNT phases according to rule of mixture.[18, 19, 21] The calculated effective modulus for TPU-CNT phase is 1804.2 MPa, 1288.4 MPa and 778 MPa for blends containing 30%, 50% and 70% TPU-CNT phase, respectively.

Therefore, the TPU-CNT phase in POE/TPU-CNT 70/30-CNT is more difficult to be deformed under strain. This is in agreement with above assumption. If such "slippage" mechanism is truly responsible for the resistivity-strain behavior observed, for CPCs containing more TPU phase (such as 50% and 70%), the relative large TPU content could lead to the fibrillization of TPU-CNT phase at relative larger strain, leading to a stable phase diameter and thus resistivity at relative larger strains. Then, the different transition strains shown in Fig. S1 can be explained by the different pre-stretching magnitude caused difference in fibrillization process for these CPCs.

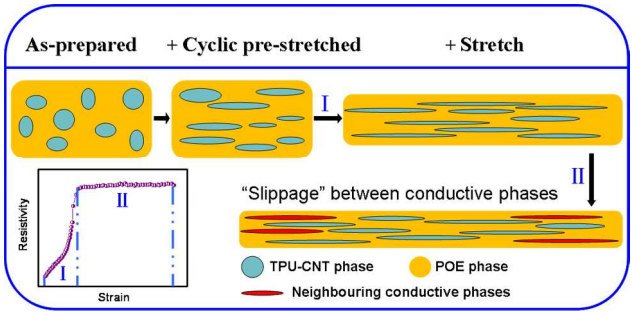

Fig. 7 The sketch of the phase morphology evolution for as-prepared, cyclic pre-stretched and subsequently stretched specimens. This demonstrates the proposed "slippage" mechanism responsible for observed resistivity-strain behavior.

4 Conclusions

Polymer blends and subsequent pre-stretching are used for the fabrication of selectively distributed and oriented conductive networks. It is observed that constant resistivity under strain can be achieved at relative low filler content (5.7 wt.%). And a tunable two-step wise resistivity-strain behavior is illustrated. To characterize the phase morphology and conductive network structure of these CPCs, contact angle measurement, SEM, Raman spectroscopy and DMA are performed. From these characterizations, it is observed that MWCNTs are selectively distributed in TPU phase. Pre-stretching process has lead to orientation of these TPU-CNT phases, and further stretching can cause fibrillization. Through monitor the orientation of MWCNTs with Raman spectroscopy, it is shown that MWCNTs orientation correlates well with the change of resistivity, and can be used as an indicator to reflect the change on conductive network. Combine the information obtained from resistivity-strain dependency, phase morphology, and conductive network morphology, the deformation and fibrillization of conductive phases are thought to be responsible for the initial increase and "slippage" between conductive phases model is proposed to explain the constant resistivity under further strain. This study provides a guideline for the preparation of high performance strain sensors as well as stretchable conductors for a number of applications.

Acknowledgements

We express our sincere thanks to the National Natural Science Foundation of China for financial support (51273117 and 51121001). This work was subsidized by the special funds for Major State Basic Research Projects of China (2011CB606006). H. Deng would like to thank the Ministry of Education (Program for New Century Excellent Talents in University, NCET-13-0383), Sichuan province for financial support (2013JQ0008) and the Innovation Team Program of Science & Technology Department of Sichuan Province (2013TD0013). S.R. Fu would like to thank the Department of Science and Technology in Sichuan province for financial support (2012RZ0006).

Notes and references

[a] *College of Polymer Science and Engineering, State Key laboratory of Polymer Materials Engineering, Sichuan University, Chengdu 610065, China. Fax: 28 8540 5401; Tel: 28 8546 1795; E-mail: qiangfu@scu.edu.cn*

1. X. Gao, S. M. Zhang, F. Mai, L. Lin, Y. Deng, H. Deng and Q. Fu, *Journal of Materials Chemistry*, 2011, **21**, 6401-6408.
2. L. Chen, G. Chen and L. Lu, *Advanced Functional Materials*, 2007, **17**, 898-904.
3. H. Deng, T. Skipa, E. Bilotti, R. Zhang, D. Lellinger, L. Mezzo, Q. Fu, I. Alig and T. Peijs, *Advanced Functional Materials*, 2010, **20**, 1424-1432.
4. I. Alig, D. Lellinger, M. Engel, T. Skipa and P. Potschke, *Polymer*, 2008, **49**, 1902-1909.
5. L. Chang, K. Friedrich, L. Ye and P. Toro, *J. Mater. Sci.*, 2009, **44**, 4003-4012.
6. L. Lin, S. Y. Liu, Q. Zhang, X. Y. Li, M. Z. Ji, H. Deng and Q. Fu, *ACS Appl. Mater. Interfaces*, 2013, **5**, 5815-5824.
7. L. Gao, E. T. Thostenson, Z. Zhang and T.-W. Chou, *Advanced Functional Materials*, 2009, **19**, 123-130.
8. K. H. Kim, M. Vural and M. F. Islam, *Adv. Mater.*, 2011, **23**, 2865-2869.
9. V. Eswaraiah, K. Balasubramaniam and S. Ramaprabhu, *Journal of Materials Chemistry*, 2011, **21**, 12626-12628.
10. K. S. Kim, Y. Zhao, H. Jang, S. Y. Lee, J. M. Kim, K. S. Kim, J.-H. Ahn, P. Kim, J.-Y. Choi and B. H. Hong, *Nature*, 2009, **457**, 706-710.
11. Z. Chen, W. Ren, L. Gao, B. Liu, S. Pei and H.-M. Cheng, *Nature Materials*, 2011, **10**, 424-428.
12. I. Alig, T. Skipa, M. Engel, D. Lellinger, S. Pegel and P. Potschke, *Physica Status Solidi B-Basic Solid State Physics*, 2007, **244**, 4223-4226.
13. D. F. Wu, Y. S. Zhang, M. Zhang and W. Yu, *Biomacromolecules*, 2009, **10**, 417-424.
14. A. Goeldel, A. Marmur, G. R. Kasaliwal, P. Poetschke and G. Heinrich, *Macromolecules*, 2011, **44**, 6094-6102.
15. M. Z. Ji, H. Deng, D. X. Yan, X. Y. Li, L. Y. Duan and Q. Fu, *Composites Science and Technology*, 2014, **92**, 16-26.
16. L. Lin, S. Y. Liu, S. Y. Fu, S. M. Zhang, H. Deng and Q. Fu, *Small*, 2013, **9**, 3620-3629.
17. S. M. Miriyala, Y. S. Kim, L. Liu and J. C. Grunlan, *Macromolecular Chemistry and Physics*, 2008, **209**, 2399-2409.
18. T. G. Mason, M. D. Lacasse, G. S. Grest, D. Levine, J. Bibette and D. A. Weitz, *Physical Review E*, 1997, **56**, 3150-3166.
19. S. Ikeda, E. A. Foegeding and T. Hagiwara, *Langmuir*, 1999, **15**, 8584-8589.
20. G. Jihua, B. Minaie, B. Wang, L. Zhiyong and C. Zhang, *Computational Materials Science*, 2004, **31**, 225-236.
21. M. Idicula, S. K. Malhotra, K. Joseph and S. Thomas, *Composites Science and Technology*, 2005, **65**, 1077-1087.
22. N. D. Alexopoulos, C. Bartholome, P. Poulin and Z. Marioli-Riga, *Composites Science and Technology*, 2010, **70**, 260-271.

23. K. Yoonseob, Z. Jian, Y. Bongjun, M. Di Prima, S. Xianli, K. Jin-Gyu, Y. Seung Jo, C. Uher and N. A. Kotov, *Nature*, 2013, **500**, 59-64.
24. T. Sekitani, Y. Noguchi, K. Hata, T. Fukushima, T. Aida and T. Someya, *Science*, 2008, **321**, 1468-1472.
25. P. Slobodian, P. Riha and P. Saha, *Carbon*, 2012, **50**, 3446-3453.
26. Y. Shang, X. He, Y. Li, L. Zhang, Z. Li, C. Ji, E. Shi, P. Li, K. Zhu, Q. Peng, C. Wang, X. Zhang, R. Wang, J. Wei, K. Wang, H. Zhu, D. Wu and A. Cao, *Adv. Mater.*, 2012, **24**, 2896-2900.
27. T. Sekitani, H. Nakajima, H. Maeda, T. Fukushima, T. Aida, K. Hata and T. Someya, *Nature Materials*, 2009, **8**, 494-499.
28. C. Kyoung-Yong, O. Youngseok, R. Jonghyun, A. Jong-Hyun, K. Young-Jin, C. Hyouk Ryeol and B. Seunghyun, *Nature Nanotechnology*, 2010, **5**, 853-857.
29. T. Yamada, Y. Hayamizu, Y. Yamamoto, Y. Yomogida, A. Izadi-Najafabadi, D. N. Futaba and K. Hata, *Nature Nanotechnology*, 2011, **6**, 296-301.
30. J. Hwang, J. Jang, K. Hong, K. N. Kim, J. H. Han, K. Shin and C. E. Park, *Carbon*, 2011, **49**, 106-110.
31. Z.-M. Dang, M.-J. Jiang, D. Xie, S.-H. Yao, L.-Q. Zhang and J. Bai, *J. Appl. Phys.*, 2008, **104**, 024114.
32. R. Zhang, M. Baxendale and T. Peijs, *Phys. Rev. B*, 2007, **76**, 195433.
33. L. Lin, H. Deng, X. Gao, S. M. Zhang, E. Bilotti, T. Peijs and Q. Fu, *Polymer International*, 2013, **62**, 134-140.
34. A. Goeldel, G. Kasaliwal and P. Poetschke, *Macromolecular Rapid Communications*, 2009, **30**, 423-429.
35. P. Poetschke, S. Pegel, M. Claes and D. Bonduel, *Macromolecular Rapid Communications*, 2008, **29**, 244-251.
36. D. Wu, D. Lin, J. Zhang, W. Zhou, M. Zhang, Y. Zhang, D. Wang and B. Lin, *Macromolecular Chemistry and Physics*, 2011, **212**, 613-626.
37. M. Wu and L. L. Shaw, *Journal of Power Sources*, 2004, **136**, 37-44.
38. A. Goldel, A. Marmur, G. R. Kasaliwal, P. Potschke and G. Heinrich, *Macromolecules*, 2011, **44**, 6094-6102.
39. A. C. Baudouin, C. Bailly and J. Devaux, *Polym. Degrad. Stabil.*, 2010, **95**, 389-398.
40. A.-C. Baudouin, J. Devaux and C. Bailly, *Polymer*, 2010, **51**, 1341-1354.
41. F. Fenouillot, P. Cassagnau and J. C. Majeste, *Polymer*, 2009, **50**, 1333-1350.
42. Z. Shuangmei, L. Lin, D. Hua, G. Xiang, E. Bilotti, T. Peijs, Z. Qin and F. Qiang, *Colloid and Polymer Science*, 2012, **290**, 1393-1401.

